

A Multisite Decomposition of the Tensor Network Path Integrals

Amartya Bose*

Department of Chemistry, Princeton University, Princeton, New Jersey 08544

Peter L. Walters*

*Department of Chemistry, University of California, Berkeley, California 94720 and
Miller Institute for Basic Research in Science, University of California Berkeley, Berkeley, California 94720*

Tensor network decompositions of path integrals for simulating open quantum systems have recently been proven to be useful. In this work, we extend the tensor network path integral (TNPI) framework to efficiently simulate extended systems coupled with local vibrational and phononic modes. The Feynman-Vernon influence functional is a very popular approach used to account for the effect of a bath on the dynamics of the system. In order to facilitate the incorporation of the influence functional into a multisite framework (MS-TNPI), we combine a matrix product state decomposition of the reduced density tensor of the system along the sites with a corresponding tensor network representation of the time axis to construct an efficient 2D tensor network. The 2D MS-TNPI network, when finally contracted, yields the time-dependent reduced density tensor of the extended system as a matrix product state. The decomposition and algorithm presented are independent of the nature of the system Hamiltonian. We also outline an iteration scheme to take the simulation beyond the non-Markovian memory length introduced by the dissipative baths. Applications to spin chains coupled to local harmonic baths is presented; we consider interactions defined by the Ising, XXZ and the Heisenberg models. We demonstrate that the presence of dissipative environments can often dissipate the entanglement between the sites as measured by the bond dimension of the reduced density matrix product state. The MS-TNPI method would be useful for studying a variety of extended quantum systems coupled with vibrational baths or phononic modes.

I. INTRODUCTION

Quantum effects in dynamics are very important for studying charge or exciton energy transfer in long chains and in understanding decoherence in systems of qubits. To curtail the exponential growth of computational complexity, a system-solvent description is often used. While in many cases it is indeed possible to limit the quantum description to only a small subspace of degrees of freedom, for extended systems however, this quantum subspace or “system” can be quite large. Thus, the effectiveness of a typical system-solvent decomposition might be compromised. Methods like density matrix renormalization group [1–4] (DMRG) and its time-dependent variant [5–7] (tDMRG) are very useful in simulating these large systems by decomposing the wave function along the “system” axis using sequential singular value decompositions (SVD). Multiconfiguration time-dependent Hartree (MCTDH) and its multi-level version (ML-MCTDH) constitute another family of tensor network-based algorithms that have also been commonly used to simulate non-equilibrium dynamics. However, when vibrational or phononic modes are present, the wave function-based nature of these algorithms pose significant computational challenges. Also, strictly speaking, a proper description of thermal equilibrium is not truly possible using a wave function-based method [8].

Propagating the reduced density matrix for the “system” is a lucrative option for simulating open quantum

systems. Path integrals based on the Feynman-Vernon influence functional (IF) [9] and the hierarchical equations of motion (HEOM) [10] are rigorous methods for incorporating the interactions between systems and solvents without having to simulate the vibrational manifold explicitly. While HEOM is, in principle, exact for systems interacting with arbitrary harmonic baths, practically, it has been mostly restricted to simulating the case of baths described by a Drude spectral densities. Attempts have been made to develop efficient HEOM-based algorithms that are applicable to general spectral densities [8, 10–13]. In case the solvent is atomistically defined and anharmonic effects are important, the IF does not have a closed-form expression. Classical trajectories are often used for estimating the influence functional in such cases [14–18]. The quasi-adiabatic propagator path integrals (QuAPI) [19, 20] and related methods [21–23] are useful when simulating systems bilinearly coupled to harmonic baths. Recently, tensor networks have also been shown to be useful in making calculations with influence functionals more efficient [24–29].

Simulating thermal dynamics of extended systems coupled to a vibrational manifold poses unique challenges. As mentioned before, even though there have been attempts to incorporate the bath in terms of a basis set [30], wave function-based methods like DMRG or tDMRG are typically not well-suited. The computational complexity tends to grow because of the entanglement between the system states and the bath modes. Path integral-based methods have also been developed to account for extended systems with short-ranged interactions [31–34]. Based on tensor network decompositions, Lerose *et al.*

* Both authors contributed equally to this work.

[35] have developed a method for simulating influence functionals for cases where the system and the environment are made of indistinguishable particles. In particular, they applied their method to calculate the reduced density matrix for a specific site in a spin-chain.

Tensor network path integrals (TNPI) [28] offer an approach to influence functional-based path integral simulations that can, quite naturally, be extended to handle problems involving extended systems interacting with localized solvents. TNPI typically involves a matrix product (MP) representation of the ‘‘augmented propagator’’ (AP). Here, we extend this representation to account for multiple system sites (or particles) leading to a multi-site version of the TNPI framework (MS-TNPI). The resulting two-dimensional tensor network can be efficiently contracted and used to simulate the reduced dynamics (in terms of a MP representation) of the extended system. From a different perspective, MS-TNPI can be thought of as an extension of tDMRG that incorporates Feynman-Vernon influence functionals to account for interactions of sites with local solvents.

As we will show, the MS-TNPI framework is independent of the structure of the system Hamiltonian. All it requires is a matrix product operator (MPO) representation of the propagator. Thus, long-ranged interactions can be accounted for without any change to the fundamental structure of the problem. The time-evolved reduced density tensor corresponding to the entire extended system is directly evaluated in the form of a matrix product state (MPS). The method is implemented using the open-source ITensor library [36]. In Sec. II, we develop the structure of MS-TNPI. The method is illustrated with some examples in Sec. III. Finally, we end the paper with some concluding remarks and future prospects in Sec. IV.

II. METHODOLOGY

Consider a system consisting of P particles or sites each with its local vibrational degrees of freedom:

$$\hat{H} = \hat{H}_0 + \sum_{i=1}^P \hat{V}_i, \quad (1)$$

where \hat{H}_0 is the system Hamiltonian and \hat{V}_i is the Hamiltonian encoding the system-vibration interaction localized on the i^{th} site.

The site-vibration interactions generally have anharmonic terms, but under Gaussian response theory, the effect of the anharmonic vibrations can be accounted for by an equivalent harmonic bath on the i^{th} site:

$$\hat{V}_i = \sum_{l=1}^N \frac{p_{i,l}^2}{2m_{j,l}} + \frac{1}{2} m_{i,l} \omega_{i,l}^2 \left(x_{i,l} - \frac{c_{i,l} \hat{s}_i}{m_{i,l} \omega_{i,l}^2} \right)^2, \quad (2)$$

where $\omega_{i,l}$ and $c_{i,l}$ are the frequency and coupling of the l^{th} mode of the i^{th} site, respectively. Additionally,

\hat{s}_i is the system operator, associated with the i^{th} site, that couples the site with its local vibrations. The site-vibration interaction is characterized by a spectral density [37, 38]:

$$J(\omega) = \frac{\pi}{2} \sum_l \frac{c_l^2}{m_l \omega_l} \delta(\omega - \omega_l). \quad (3)$$

In case the vibrations are defined by atomistic Hamiltonians, it is often possible to obtain the spectral density as a Fourier transform of the energy-gap autocorrelation function obtained via classical trajectory simulations. In case of interactions with phonons, typically the modes can be exactly described by harmonic oscillators even without invoking Gaussian response theory.

The reduced dynamics of a system coupled to a harmonic bath is given by

$$\begin{aligned} \tilde{\rho}(S_N^\pm, N\Delta t) &= \text{Tr}_{\text{bath}} \langle S_N^+ | \rho(N\Delta t) | S_N^- \rangle \\ &= \sum_{S_0^\pm} \tilde{\rho}(S_0^\pm, 0) G(S_0^\pm, S_N^\pm, N\Delta t), \end{aligned} \quad (4)$$

where $\tilde{\rho}$ is the system’s reduced density tensor and G is the AP. In this notation, S_j^\pm represents the forward-backward state of all the sites at the j^{th} time point, with the state of the i^{th} site at this time point being denoted by $s_{i,j}^\pm$. In the absence of any coupling between the system and the bath, the bare AP is given by:

$$G^{(0)}(S_0^\pm, S_N^\pm, N\Delta t) = \sum_{S_1^\pm} \cdots \sum_{S_{N-1}^\pm} P_{S_0^\pm \dots S_N^\pm}^{(0)}, \quad (5)$$

with

$$P_{S_0^\pm \dots S_N^\pm}^{(0)} = K(S_0^\pm, S_1^\pm, \Delta t) \times \cdots \times K(S_{N-1}^\pm, S_N^\pm, \Delta t). \quad (6)$$

Here, $P_{S_0^\pm \dots S_N^\pm}^{(0)}$ is the bare path amplitude tensor and $K(S_n^\pm, S_{n+1}^\pm, \Delta t)$ is the forward-backward propagator (i.e. the direct product of the forward and backward propagators) connecting the system at the n^{th} time point to the $(n+1)^{\text{th}}$ time point. From Eqs. (5) and (6), we see that without the bath, the bare propagator, $G^{(0)}$, and thus, the reduced dynamics can be evaluated iteratively. The bath’s presence, however, introduces non-Markovian effects that prevent such a straightforward evaluation of the dynamics.

The dynamics of a system coupled to a harmonic bath is well-described by the formalism of Feynman-Vernon influence functionals (IF). In this formalism, the AP is given by the following equations [19, 20]:

$$G(S_0^\pm, S_N^\pm, N\Delta t) = \sum_{S_1^\pm} \cdots \sum_{S_{N-1}^\pm} P_{S_0^\pm \dots S_N^\pm} \quad (7)$$

$$= \sum_{S_1^\pm} \cdots \sum_{S_{N-1}^\pm} F[\{S_j^\pm\}] P_{S_0^\pm \dots S_N^\pm}^{(0)} \quad (8)$$

where $P_{S_0^\pm \dots S_N^\pm}$ is the path amplitude tensor and $F[\{S_j^\pm\}]$ is the influence functional for the given forward-backward system path. The path amplitude tensor, has $O(d^{2NP})$ coefficients, where d is the dimensionality of a typical system site, N is the number of time points and P is the number of sites. The number of coefficients grows exponentially with both the number of sites as well as the number of time points. In this work, we aim to combat this exponential growth, by factorizing this unmanageably large tensor into a 2D network of smaller ones.

We start by representing the forward-backward propagator, K , in the form of a matrix product operator (MPO),

$$K(S_n^\pm, S_{n+1}^\pm \Delta t) = \sum_{\{\alpha(i,n)\}} W_{\alpha(1,n)}^{s_{1,n}^\pm, s_{1,n+1}^\pm} W_{\alpha(1,n), \alpha(2,n)}^{s_{2,n}^\pm, s_{2,n+1}^\pm} \dots W_{\alpha(P-2,n), \alpha(P-1,n)}^{s_{P-1,n}^\pm, s_{P-1,n+1}^\pm} W_{\alpha(P-1,n)}^{s_{P,n}^\pm, s_{P,n+1}^\pm}. \quad (9)$$

Here, a typical ‘‘site’’ index, $s_{i,j}^\pm$, has two subscripts: the first subscript, i , is for the site (or particle) number and the second one, j , indicates the time point. The parentheses on the the bond indices, $\alpha(i,n)$, are only included for visual clarity. Loosely speaking, the tensor, $W_{\alpha(i-1,n), \alpha(i,n)}^{s_{i,n}^\pm, s_{i,n+1}^\pm}$, can be thought of as an effective forward-backward propagator acting on the i^{th} site.

In principle any forward-backward propagator can be represented as a MPO, but doing so may be as costly as directly solving the Schrödinger equation. Fortunately, using matrix product representations for studying dynamics of the bare system has been a topic of intense research over the years. Various methods like time-evolving block decimation (TEBD) [5, 39, 40] and time-dependent DMRG (tDMRG) [5, 7] have been developed to directly simulate the time evolution of wave functions of extended systems with short-ranged interactions. For systems with long-ranged interactions, the recently introduced MPO $W^{1,\text{II}}$ method [41] can generate very efficient representations of the propagator. Additionally, a time-dependent variational principle (TDVP) [42–44] approach has also been developed that allows for the treatment of arbitrary Hamiltonians. While TEBD and MPO $W^{1,\text{II}}$ calculate the propagators, Krylov subspace-based methods and TDVP often approximate the action of the propagator on the wave function. Detailed comparisons of these methods for the purposes of simulating the propagator, especially in the context of the current method, is extremely interesting and beyond the scope of this paper. A thorough study of these ideas would be conducted in the future. For the current development, we will simply assume that a MPO representation of the forward-backward propagator is available.

In the standard TNPI framework [24, 25, 27, 28], a temporal factorization is performed, enabling us to represent the path amplitude tensor as a MPS. In this spirit,

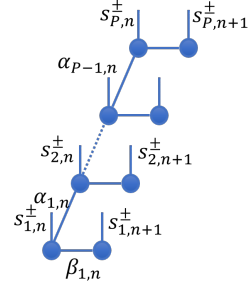


FIG. 1. Factorization of the forward-backward MPO following Eqs. (10)–(12)

we proceed by using SVD to factor the forward-backward propagator MPO:

$$W_{\alpha(1,n)}^{s_{1,n}^\pm, s_{1,n+1}^\pm} = \sum_{\beta(1,n)} L_{\alpha(1,n), \beta(1,n)}^{s_{1,n}^\pm} R_{\beta(1,n)}^{s_{1,n+1}^\pm} \quad (10)$$

$$W_{\alpha(i-1,n), \alpha(i,n)}^{s_{i,n}^\pm, s_{i,n+1}^\pm} = \sum_{\beta(i,n)} L_{\alpha(i-1,n), \alpha(i,n), \beta(i,n)}^{s_{i,n}^\pm} R_{\beta(i,n)}^{s_{i,n+1}^\pm}, \quad 1 < i < P \quad (11)$$

$$W_{\alpha(P-1,n)}^{s_{P,n}^\pm, s_{P,n+1}^\pm} = \sum_{\beta(P,n)} L_{\alpha(P-1,n), \beta(P,n)}^{s_{P,n}^\pm} R_{\beta(P,n)}^{s_{P,n+1}^\pm}. \quad (12)$$

The bonds along the ‘‘spatial’’ dimension are denoted by α , and β represents the bonds along the ‘‘temporal’’ dimension. Figure 1 shows this structure in the form of a tensor diagram.

As we mentioned earlier, the goal, here, is to express the path amplitude tensor as a 2D tensor network with time on one axis and system site on the other. The presence of the IF complicates matters. Therefore, let us first derive the expressions corresponding to the the bare path amplitude tensor. First, we plug Eqs. (10)–(12) into Eq. (9), then substitute the resulting expression into Eq. (6). After grouping terms by time point, we see that the tensors corresponding to the the initial point are given as:

$$M_{\alpha(1,0), \beta(1,0)}^{s_{1,0}^\pm} = L_{\alpha(1,0), \beta(1,0)}^{s_{1,0}^\pm} \quad (13)$$

$$M_{\alpha(i,0), \beta(i,0), \alpha(i-1,0)}^{s_{i,0}^\pm} = L_{\alpha(i-1,0), \alpha(i,0), \beta(i,0)}^{s_{i,0}^\pm} \quad (14)$$

$$M_{\alpha(P-1,0), \beta(P,0)}^{s_{P,0}^\pm} = L_{\alpha(P-1,0), \beta(P,0)}^{s_{P,0}^\pm}. \quad (15)$$

The expressions for the final point:

$$M_{\beta(1,N-1)}^{s_{1,N}^\pm} = R_{\beta(1,N-1)}^{s_{1,N}^\pm} \quad (16)$$

$$M_{\beta(i,N-1)}^{s_{i,N}^\pm} = R_{\beta(i,N-1)}^{s_{i,N}^\pm} \quad (17)$$

$$M_{\beta(P,N-1)}^{s_{P,N}^\pm} = R_{\beta(P,N-1)}^{s_{P,N}^\pm}. \quad (18)$$

Lastly, for an intermediate time point, n :

$$M_{\alpha(1,n), \beta(1,n), \beta(1,n-1)}^{s_{1,n}^\pm} = R_{\beta(1,n-1)}^{s_{1,n}^\pm} L_{\alpha(1,n), \beta(1,n)}^{s_{1,n}^\pm} \quad (19)$$

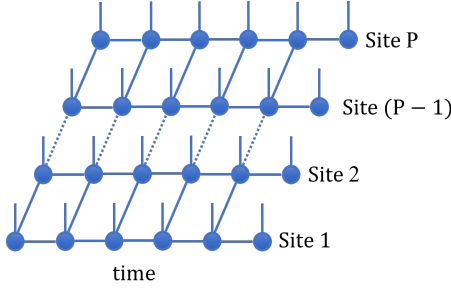


FIG. 2. Factorization of the forward-backward MPO.

$$M_{\alpha(i,n),\beta(i,n),\alpha(i-1,n),\beta(i-1,n)}^{s_{i,n}^{\pm}} = R_{\beta(i,n-1)}^{s_{i,n}^{\pm}} L_{\alpha(i-1,n),\alpha(i,n),\beta(i,n)}^{s_{i,n}^{\pm}} \quad (20)$$

$$M_{\beta(P,n),\alpha(P-1,n),\beta(P-1,n)}^{s_{P,n}^{\pm}} = R_{\beta(P,n-1)}^{s_{P,n}^{\pm}} L_{\alpha(P-1,n),\beta(P,n)}^{s_{P,n}^{\pm}}. \quad (21)$$

Putting these M tensors together, we get the 2D structure illustrated in Fig. 2. Notice that here, the sites on the final time point are not connected together, Eqs. (16)–(18), inheriting the fundamental asymmetry between the initial and final time points in the structure in Fig. 1.

The flexibility of this factorization becomes apparent when the bath interactions, in form of an IF, are incorporated. The 2D structure discussed till now can be thought of as a series of generalized tensor products along the “columns” that represent the state of the full system at a given time point, or along the “rows” that represent the state of one site at all times (i.e. the AP of that particular site). While thinking of it as a collection of columns manifestly links the method to its tDMRG heritage, its identification as a collection of “row” tensors serve to illustrate how this multisite method is related to AP-TNPI [28]. If there was no interaction between the systems, the rows would separate out and every site would behave like the standard TNPI method. This makes it quite simple to take the influence functional into account.

Because we are considering site-local baths, the total IF is just a product of the IFs on each of the sites. Since the structure of the IF is the same irrespective of the site, consider the i^{th} site. If the path of the site is given by $\{s_{i,j}^{\pm}\}$, then the IF [9] is:

$$F[\{s_{i,j}^{\pm}\}] = \exp\left(-\frac{1}{\hbar} \sum_{0 \leq k \leq N} \Delta s_{i,k} \sum_{0 \leq k' \leq k} (\text{Re}(\eta_{kk'}) \Delta s_{i,k'} + 2i \text{Im}(\eta_{kk'}) \bar{s}_{i,k'})\right) \quad (22)$$

where $\Delta s_{i,k} = s_{i,k}^+ - s_{i,k}^-$ and $\bar{s}_{i,k} = \frac{s_{i,k}^+ + s_{i,k}^-}{2}$ and $\eta_{kk'}$ are the discretized η -coefficients [19, 20]. It is possible to have different baths associated with different sites leading to a site-dependent η -coefficient and site-dependent

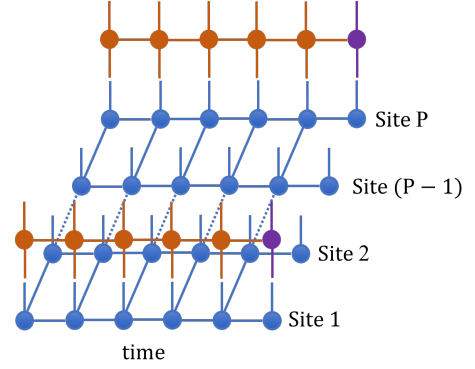


FIG. 3. Schematic showing the application of the influence functional MPO to the 2D MS-TNPI structure. Only the influence functionals for the first and the last sites are shown here. Purple vertices correspond to the “projection” operator on the last time point (cf. Ref [28]).

influence functional, however for notational convenience, we describe the method assuming the baths on different sites are characterized by the same spectral density.

We have already discussed the analytical form for the matrix product operator for the IF [28]. Following that procedure, Eq. (22) is factorized based on the k time point:

$$F_k[\{s_{i,j}^{\pm}\}] = \exp\left(-\frac{1}{\hbar} \Delta s_{i,k} \sum_{0 \leq k' \leq k} (\text{Re}(\eta_{kk'}) \Delta s_{i,k'} + 2i \text{Im}(\eta_{kk'}) \bar{s}_{i,k'})\right) \quad (23)$$

and each F_k is given an MPO-representation, \mathbb{F}_k . The MPOs are applied to each row of the 2D multisite TNPI structure for each system site in order of increasing k as detailed in Ref. [28]. The operations on the first and the last row or site is schematically indicated in Fig. 3.

The resulting tensor network corresponds to the path amplitude tensor. By tracing over the internal system indices as well as contracting all the β bonds, we can obtain the AP expressed as a MPO. This is achieved most easily by considering the network as a sequence of columns, each representing the state of the system at a given time point. Tracing over the internal system indices turns these columns into MPOs. From here, the AP MPO is obtained by multiplying all the column MPOs together in a sequential manner, thereby contracting the β bonds. By applying this AP MPO to a MPS representing the initial state of the system, we can obtain the corresponding time-evolved final state. This AP-formulation is particularly helpful if we are interested in studying the behaviors of a variety of different initial states. However, usually only the dynamics arising from a specific initial system state is desired. In such cases, we can obtain the resulting final state in a computationally efficient manner by reducing the problem to the sequential application

of the column MPOs to the initial state MPS. As MPS-MPO operations are much cheaper than MPO-MPO operations, the AP MPO should not be computed unless it is required. For the examples given here, we will restrict our attention to the MPS-MPO contraction scheme.

It is well-known that for simulations in the condensed phase, the non-Markovian memory does not extend for all of history. This means that the paths can be truncated after L time steps, to simulate a non-Markovian memory of time-span $L\Delta t$. To develop such an iteration procedure, one needs to know the full state of the system at any time point. We have access to that information for the extended system in the form of the corresponding column in the 2D lattice structure, Fig. 2. Iteration can also be done in two ways — for the AP as done in Ref. [28], or as typically done, for a particular initial state [19, 20]. Once again in the interest of simplicity of discussion and computational efficiency, we describe the iteration scheme for a particular initial reduced density tensor, C_0 . For a simulation with memory length L in the iterative regime, there would always be $L + 1$ columns, C_j for $1 \leq j \leq L + 1$. The iterative procedure is outlined below. A tensor contraction is represented by \otimes .

1. Update C_0 by applying the MPO, C_1 to it. $C_0 \leftarrow C_1 \otimes C_0$.
2. Copy the other columns in by “sliding them” back by one. $C_j \leftarrow C_{j+1}$ for $j < L$.
Notice at this stage that the new first column is no longer a MPO.
3. Update the second last column, C_L by multiplying by the corresponding L tensors.
4. Insert the last column according to Eqs. (16)–(18).
5. Apply the IF MPO in a row-wise fashion.
6. Trace over the site indices of C_1 to obtain an MPO in the first column.

The salient ideas of the iterative procedure is schematically outlined in Fig. 4.

Finally, given the immense difficulty of the problem at hand, it is of interest to estimate the complexity of the algorithm outlined. The two most computationally demanding operations that occur during each time step are the application of the IF MPO and the contraction of the resulting tensor network. Roughly speaking, the cost of applying the IF MPO is $\mathcal{O}(m_t^3 w_p^2 w_I^2 d^2 LP)$ and cost of the contraction is $\mathcal{O}(m^3 w_p^2 m_t LP)$. Here, m_t is the typical bond dimension along the time axes (i.e., a row), m is the typical bond dimension of the contracting MPS, w_I is the typical bond dimension of the IF MPO. The typical bond dimension of the forward-backward propagator of the bare system is denoted by w_p , d is the dimensionality of a typical system site and P is the number of system sites. L is the non-Markovian memory length. It is clear from the scaling that both the terms are linear in L and P . Though the magnitude of m_t might

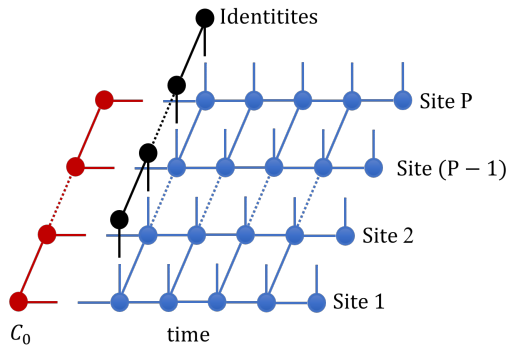


FIG. 4. Iteration of the MS-TNPI network. At step (5), notice that the first column is not a MPO. After contraction with identity MPS, it becomes a MPO.

be dependent on the memory length, L , the exponential growth of complexity within memory is effectively curtailed [28]. Since the local vibrational baths would typically consist of high frequency modes (implying that the non-Markovian memory length, L , is not very large), and the site-site couplings would be quite high, the cost would probably be dominated by the contraction process. However, if the local baths are very strongly coupled, the temporal bond dimension would grow much faster than the bond dimension along the system axis, and the pattern would be reversed.

III. RESULTS

For the purposes of illustrating the multisite TNPI method, we consider spin chains with nearest-neighbor intersite coupling. The Hamiltonian is given as

$$\hat{H}_0 = \sum_{j=1}^P \hat{h}_j^{(1)} + \sum_{j=1}^{P-1} \hat{h}_{j,j+1}^{(2)} \quad (24)$$

where

$$\hat{h}_j^{(1)} = \epsilon \hat{\sigma}_z^{(j)} - \hbar \Omega \hat{\sigma}_x^{(j)} \quad (25)$$

is the one-body term. The strength of the transverse field is Ω , and ϵ represents any asymmetry present in the system due to a longitudinal field. The two-body interaction term is given by a general nearest-neighbor Hamiltonian:

$$\hat{h}_{j,l}^{(2)} = \delta_{l,j+1} \left(J_x \hat{\sigma}_x^{(j)} \hat{\sigma}_x^{(l)} + J_y \hat{\sigma}_y^{(j)} \hat{\sigma}_y^{(l)} + J_z \hat{\sigma}_z^{(j)} \hat{\sigma}_z^{(l)} \right). \quad (26)$$

Here, $\hat{\sigma}_x^{(j)}$, $\hat{\sigma}_y^{(j)}$, $\hat{\sigma}_z^{(j)}$ are the Pauli spin matrices on the j^{th} site. Each of the sites is also coupled with its vibrational degrees of freedom described by the harmonic bath given in Eq. (2). For the examples shown here, the harmonic bath is characterized by an Ohmic spectral density with

an exponential decay:

$$J(\omega) = \frac{\pi}{2} \hbar \xi \omega \exp\left(-\frac{\omega}{\omega_c}\right) \quad (27)$$

where ξ is the dimensionless Kondo parameter, and ω_c is the characteristic cutoff frequency. In Appendix A, we outline the second-order Suzuki-Trotter splitting TEBD scheme used here to construct the forward-backward propagator MPO.

Depending on the nature of the intersite coupling, there are many models for interacting spin chains. Here, we consider the dynamics of the Ising model, the XXZ model and the Heisenberg model with $P = 31$ sites, coupled to site-local harmonic baths. The states of each

system site are labeled $|+1\rangle$ and $| -1\rangle$ which are eigenstates of the $\hat{\sigma}_z$ operator with eigenvalue of $+1$ and -1 respectively. Though the initial condition for MS-TNPI can be any arbitrary reduced density MPS (for example, a DMRG ground state), here for simplicity, it is defined as the direct product state of all spins being in $|+1\rangle$. A SVD compression scheme with a truncation threshold of χ , which is treated as a convergence parameter, is applied to the propagator MPO as well as the results of any MPS-MPO multiplications. With this scheme, singular values, λ_n , are discarded such that

$$\frac{\sum_{n \in \text{discarded}} \lambda_n^2}{\sum_n \lambda_n^2} < \chi. \quad (28)$$

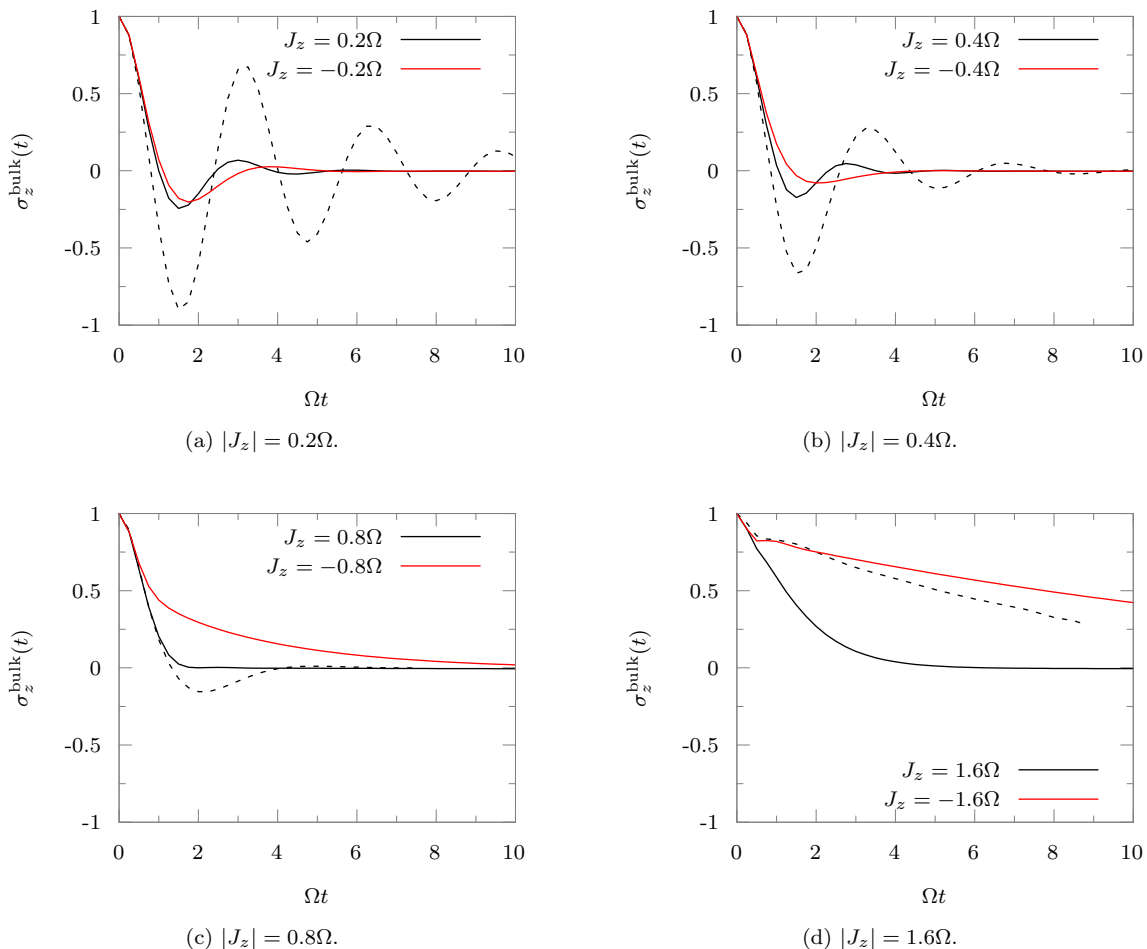


FIG. 5. Dynamics of a spin in the bulk as represented by $\langle \hat{\sigma}_z(t) \rangle$ for the 16th site of the Ising model coupled to an Ohmic bath. Dashed line: without bath.

A. Ising Model

We first consider a transverse-field Ising model ($J_x = J_y = 0$ and $J_z \neq 0$) coupled with local vibrations. The

longitudinal field is absent, $\epsilon = 0$, and a unit transverse field $\Omega = 1$ is applied.

The dynamics is simulated for different values of the

intersite coupling, $J_z = \pm 0.2, \pm 0.4, \pm 0.8$ and ± 1.6 . Here the bath is characterized by $\xi = 0.25$, $\omega_c = 5\Omega$, and it is held at an inverse temperature of $\hbar\beta\Omega = 1$. Figure 5 shows $\langle \hat{\sigma}_z(t) \rangle$ for the 16th spin in the chain. We observed that the finite size effects of the chain were limited only to a few edge sites and the dynamics of this middle monomer remained unaffected within the time-span of simulation, implying that this is the bulk dynamics.

A timestep of $\Delta t = 0.25$ was used. When the bath was present, a memory length of $L = 4$ was used, though acceptable convergence was already achieved at $L = 3$. The compression was done at a cutoff of $\chi = 10^{-11}$. The dynamics of the bare system is shown for the various cases in dashed lines. It, unlike the dynamics in presence of the dissipative bath, remains the same irrespective of the sign of J_z . For the bare dynamics, we could use the MS-TNPI method and it would reduce to a density matrix version of TEBD. However, for efficiency, we propagated the wave function using TEBD.

The case of $J_z = -0.2\Omega$ (Fig. 5 (a) red line) was discussed by Makri [45] for a system with 10 sites. We recover identical bulk dynamics with our method. We observe that the finite size of the chain affects more sites when J_z is larger (not shown in figure). This is because, for larger values of J_z , the sites “know” more about their neighbors, making the difference between an edge site with only one neighbor and a middle site with two neighbors more obvious. It is interesting that, though the difference of sign in the values of J does not impact the dynamics of the bare system, it leads to profound differences once the bath is coupled. Positive values of J appear to make the population dissipation faster.

There are two competing factors that contribute to the computational complexity — the non-Markovian memory caused by the presence of the bath, and the entanglement that develops between the sites as time evolves causing the bond dimension of the MPS to grow. In Fig. 6, we show the evolution of the average bond dimension of the reduced density MPS as a function of time for the parameters shown here. Though for the bare system case shown in Fig. 5, we propagated the wave function, here, for consistency, the density matrix is propagated. We notice that the average bond dimension grows faster for the bare system in comparison to all the cases with the bath, demonstrating the decohering effect brought in by the dissipative medium. Though the bath introduces a memory, it severely restricts the growth of the bond dimension. It is interesting to note that for higher values of interspin couplings, J , the difference in bond dimension between the positive and the negative values increases. This is also reflected in the fact that the dynamics becomes drastically different (cf. Fig. 5(c) and (d)). The eventual decrease in the bond dimension in the presence of a bath reflects its ability to disentangle the system states.

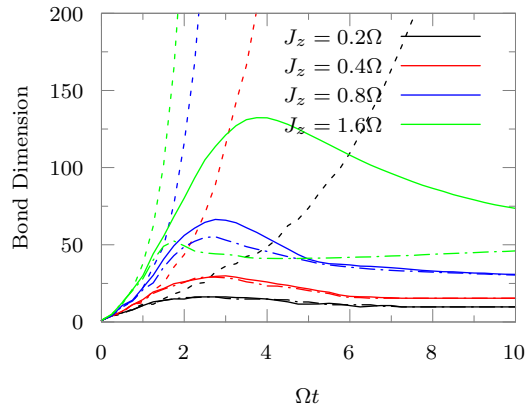


FIG. 6. Average bond dimensions of the reduced density MPS for the bare (dashed line) and the full system for various intersite couplings. Positive J is represented by the full solid line and negative J by the dot-dashed line.

B. XXZ Model

Another common model is the so-called XXZ-model, where the two-body interaction term is defined by $J_x = J_y = J \neq 0$. In absence of any external field, the ratio between J_z and J is an order parameter for quantum phase transitions at zero temperature [46]. When $J_z < -J$, the ground state is ferromagnetic. There is a disordered spin-liquid phase when $-1 < \frac{J_z}{J} < 1$, and finally for $J_z > J$, there is an antiferromagnetic state.

Here, we consider an XXZ system in an external transverse field of strength $\Omega = 1$ and with a longitudinal field of $\epsilon = 0$. The harmonic bath is once again held at an inverse temperature of $\hbar\Omega\beta = 1$. However, in these examples, it is characterized by $\xi = 0.2$, $\omega_c = 2$. We consider cases where $J_z = \pm 5J$ and $J_z = 0$. The time-step used for the convergence is $\Delta t = 0.25$. The dynamics of $\langle \hat{\sigma}_z(t) \rangle$ for a bulk spin is demonstrated for $J = 0.1$ and $J_x = 0, \pm 0.5$ in Fig. 7.

The compression was done at a cutoff of $\chi = 10^{-11}$. We note that the dynamics corresponding to the different values of J_z are totally different, even in the absence of the bath. It seems that the dissipation effects increase as the absolute value of J_z increases. However, this increase in dissipation does not happen symmetrically. The effects coming from a negative J_z is much more pronounced than those caused by a positive value. These differences and the full effects of vibrational baths are very interesting and deserve a thorough analysis, that will be the subject of future work.

C. Heisenberg Model

The most general model for interacting spin chains is the so-called “Heisenberg” model. The Hamiltonian is characterized by a two-body spin-spin interaction term

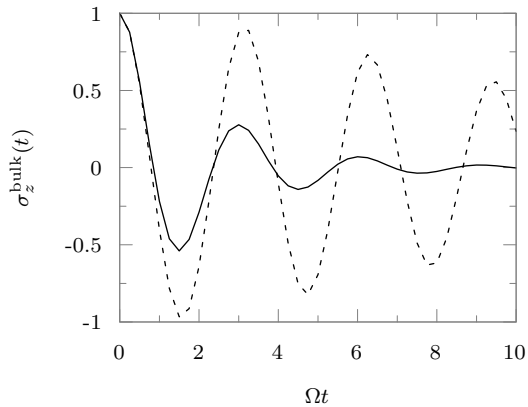
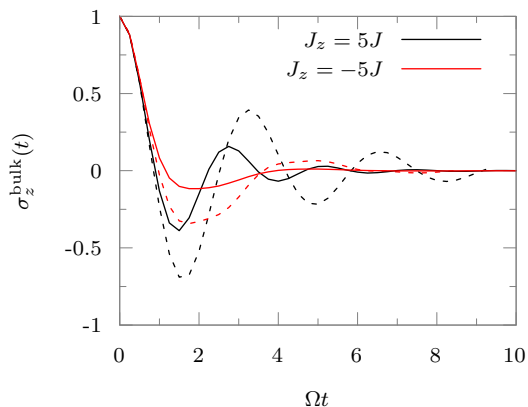
(a) $J = 0.1, J_z = 0$.(b) $J = 0.1, |J_z| = 0.5$.

FIG. 7. Dynamics of a spin in the bulk as represented by $\langle \hat{\sigma}_z(t) \rangle$ for the 16th site of the XXZ-model coupled to a harmonic bath. Dashed line: without bath.

that involves independent couplings along X , Y and Z . The bath used for this example is the same as the one used for the XXZ-model examples.

The dynamics of $\langle \hat{\sigma}_z(t) \rangle$ for a state in the bulk is shown in Fig. 8 for the case of $J_x = 0, J_y = 0.1, J_z = \pm 0.5$. The simulation was converged at a time-step of $\Delta t = 0.375$, a memory length of $L = 3$ and a cutoff of $\chi = 10^{-10}$. While we report the dynamics of only the bulk spin here, for the case of $J_z = 0.5$, our simulations reproduce the previously obtained results [34] for the terminal edge spin. It is interesting to note that, unlike the previous examples, for this Heisenberg model, the negative value of J_z results in a more oscillatory dynamics.

IV. CONCLUSION

System-solvent decomposition is used in various fields of study and is simulated using the Feynman-Vernon influence functional. In such applications there is a necessity to have a low-dimensional quantum system for com-

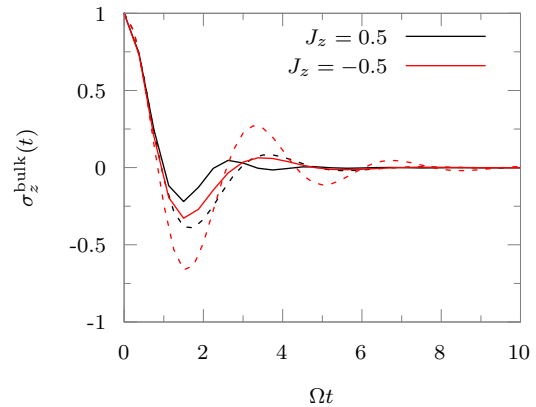


FIG. 8. Dynamics of a spin in the bulk represented by $\langle \hat{\sigma}_z(t) \rangle$ for the 16th site of the Heisenberg model coupled to a harmonic bath. Dashed line: without bath.

putational feasibility. However, many interesting problems involve extended systems that can be modeled as collection of many low-dimensional units. Typical examples involve spin-chains to model magnetism and charge or exciton transfers.

Recently, various methods based on tensor networks have been proposed to compress the path integrals, thereby reducing the storage requirements for the simulation. These tensor network path integral methods naturally suggest a further decomposition along the system dimension leading to a multisite method. In this paper, we have introduced a multisite tensor network framework called MS-TNPI. It is a 2D extension of the 1D MPS structure used in the AP-TNPI [28] or the time-evolving matrix product operators method (TEMPO) [24].

The most essential part of MS-TNPI starts with the definition of a forward-backward propagator for the extended system. This is a common problem that is extensively dealt with in the literature [5, 6, 30, 39]. We show how we can essentially use these propagators and refactorize them to obtain the current 2D structure. We also discuss how by viewing the aforementioned tensor network as a collection of rows containing the path amplitude tensors corresponding to every site, it becomes possible to now apply the influence functional MPO for the local bath in a systematic manner. Exploration of other existing methods for MPO-MPS style wave function propagation in the current context would be an interesting avenue of research. Especially methods like $W^{1,II}$ and TDVP, if adapted to the current framework, would enable the simulation of significantly long-ranged interacting systems in presence of local phononic modes.

In general, the MS-TNPI structure can be used to calculate the AP for the extended quantum system. In this paper, however, we have outlined very efficient algorithms that focus on using it to generate the full reduced density tensor corresponding to the entire extended system at any point of time in the form of a MPS. While

having this global knowledge means that the storage requirements increase with the number of sites, we show that the presence of the local vibrational bath helps decrease the growth of the bond dimension of the reduced density MPS. An added advantage of this feature is that it enables us to do memory iteration corresponding to the finiteness of the non-Markovian memory quite trivially. While the current development uses the analytical form for the influence functionals derived for harmonic baths, it would be interesting to explore the prospects of using the present structure with the more general numerical algorithm for calculating the influence functionals as MPO derived by Ye and Chan [27].

MS-TNPI is demonstrated through illustrative examples of various spin-chains coupled to local harmonic baths. We simulate the Ising model, the XXZ-model and the Heisenberg model with various different parameters. We show that the site-local baths severely restrict the growth of the bond dimension in the reduced density MPS. Consequently, in comparison to the bare system, the intersite entanglement grows slower and often even decreases in the presence of dissipative environments. There are interesting features of the dynamics for the various phases of the XXZ-model that require further investigation. This would be the subject of future work.

MS-TNPI promises to be an exciting method for extended systems. It makes it possible to study various energy and charge transfer processes, and loss of coherence in chains of qubits. Such applications shall be the focus of our research in the near future. Additionally, the novelty of the structure opens up possibilities for further improvements and developments of which we have only begun scratching the surface.

ACKNOWLEDGMENTS

A. B. acknowledges the support of the Computational Chemical Center: Chemistry in Solution and at Interfaces funded by the US Department of Energy under Award No. DE-SC0019394. P. W. acknowledges the Miller Institute for Basic Research in Science for funding.

Appendix A: System Forward-Backward Propagator in MPO representation

For the simple case of nearest-neighbor interacting Hamiltonian, it is very easy to define an algorithm for calculating the second-order Suzuki-Trotter split forward-backward propagator. This is a “forward-backward” version of the second-order time-evolved block decimation scheme [6].

Let the Hamiltonian be factorized as:

$$\hat{H}_0 = \sum_{j=1}^{P-1} \hat{\mathcal{H}}_{j,(j+1)} \quad (\text{A1})$$

where $\hat{\mathcal{H}}_{j,(j+1)}$ takes the one-body term into account as well. To get the second-order splitting, it is usual to incorporate the terminal single body terms fully into the corresponding terms. Everything else is split in halves:

$$\hat{\mathcal{H}}_{1,2} = \hat{h}_1^{(1)} + \hat{h}_{1,2}^{(2)} + \frac{1}{2}\hat{h}_2^{(1)} \quad (\text{A2})$$

$$\hat{\mathcal{H}}_{j,(j+1)} = \frac{1}{2}\hat{h}_j^{(1)} + \hat{h}_{j,(j+1)}^{(2)} + \frac{1}{2}\hat{h}_{(j+1)}^{(1)}, \quad 2 \leq j < N-1 \quad (\text{A3})$$

$$\hat{\mathcal{H}}_{(P-1),P} = \frac{1}{2}\hat{h}_{(P-1)}^{(1)} + \hat{h}_{(P-1),P}^{(2)} + \hat{h}_P^{(1)}. \quad (\text{A4})$$

Now, the terms are grouped as “even” and “odd” as follows:

$$\hat{\mathcal{H}}_{\text{odd}} = \sum_{1 \leq j < P}^{j \text{ odd}} \hat{\mathcal{H}}_{j,(j+1)} \quad (\text{A5})$$

$$\hat{\mathcal{H}}_{\text{even}} = \sum_{1 \leq j < P}^{j \text{ even}} \hat{\mathcal{H}}_{j,(j+1)}. \quad (\text{A6})$$

First, we define the two-body propagators, and separate out the system sites using a singular value decomposition:

$$\begin{aligned} U(s_{j,0}^+, s_{(j+1),0}^+, s_{j,1}^+, s_{(j+1),1}^+, \Delta t) \\ = \left\langle s_{j,1}^+, s_{(j+1),1}^+ \left| \exp \left(-\frac{i}{\hbar} \hat{\mathcal{H}}_{j,(j+1)} \Delta t \right) \right| s_{j,0}^+, s_{(j+1),0}^+ \right\rangle \\ = \sum_{\alpha_j} B_{s_{j,0}^+, s_{j,1}^+, \alpha_j} B_{\alpha_j, s_{(j+1),0}^+, s_{(j+1),1}^+} \end{aligned} \quad (\text{A7})$$

The forward-backward propagators corresponding to the even and odd parts can be formed simply by taking the direct product of the forward and backward propagator matrix elements. We just discuss the odd part for brevity:

$$\begin{aligned} K_{\text{odd}}(S_0^\pm, S_1^\pm, \Delta t) = \prod_{1 \leq j < P}^{j \text{ odd}} U(s_{j,0}^+, s_{(j+1),0}^+, s_{j,1}^+, s_{(j+1),1}^+, \Delta t) \\ \times U^\dagger(s_{j,0}^-, s_{(j+1),0}^-, s_{j,1}^-, s_{(j+1),1}^-, \Delta t) \end{aligned} \quad (\text{A8})$$

The odd and even propagators can now be used to generate the full single time-step forward-backward propagator under a second order Suzuki-Trotter factorization:

$$\begin{aligned} K(S_0^\pm, S_1^\pm, \Delta t) = \sum_{\kappa, \lambda} K_{\text{odd}}(S_0^\pm, \kappa, \frac{1}{2}\Delta t) \\ \times K_{\text{even}}(\kappa, \lambda, \Delta t) \\ \times K_{\text{odd}}(\lambda, S_1^\pm, \frac{1}{2}\Delta t). \end{aligned} \quad (\text{A9})$$

where κ and λ are the sets of forward-backward states of all the system sites at the two intermediate points. It is simple to recast Eq. (A9) into an MPO using Eq. (A7) leading to Eq. (9).

-
- [1] S. R. White, Density matrix formulation for quantum renormalization groups, *Phys. Rev. Lett.* **69**, 2863 (1992).
- [2] U. Schollwöck, The density-matrix renormalization group, *Rev. Mod. Phys.* **77**, 259 (2005).
- [3] U. Schollwöck, The density-matrix renormalization group: A short introduction, *Philos. Trans. A Math. Phys. Eng. Sci.* **369**, 2643 (2011).
- [4] U. Schollwöck, The density-matrix renormalization group in the age of matrix product states, *Ann. Phys. (N. Y.)* **326**, 96 (2011).
- [5] S. R. White and A. E. Feiguin, Real-Time Evolution Using the Density Matrix Renormalization Group, *Phys. Rev. Lett.* **93**, 10.1103/physrevlett.93.076401 (2004).
- [6] S. Paeckel, T. Köhler, A. Swoboda, S. R. Manmana, U. Schollwöck, and C. Hubig, Time-evolution methods for matrix-product states, *Ann. Phys. (N. Y.)* **411**, 167998 (2019).
- [7] X. Xie, Y. Liu, Y. Yao, U. Schollwöck, C. Liu, and H. Ma, Time-dependent density matrix renormalization group quantum dynamics for realistic chemical systems, *J. Chem. Phys.* **151**, 224101 (2019).
- [8] Y. Tanimura, Numerically “exact” approach to open quantum dynamics: The hierarchical equations of motion (HEOM), *J. Chem. Phys.* **153**, 020901 (2020).
- [9] R. P. Feynman and F. L. Vernon, The theory of a general quantum system interacting with a linear dissipative system, *Ann. Phys. (N. Y.)* **24**, 118 (1963).
- [10] Y. Tanimura and R. Kubo, Time Evolution of a Quantum System in Contact with a Nearly Gaussian-Markoffian Noise Bath, *J. Phys. Soc. Jpn.* **58**, 101 (1989).
- [11] C. Duan, Q. Wang, Z. Tang, and J. Wu, The study of an extended hierarchy equation of motion in the spin-boson model: The cutoff function of the sub-Ohmic spectral density, *J. Chem. Phys.* **147**, 164112 (2017).
- [12] T. Ikeda and G. D. Scholes, Generalization of the hierarchical equations of motion theory for efficient calculations with arbitrary correlation functions, *J. Chem. Phys.* **152**, 204101 (2020).
- [13] B. Popescu, H. Rahman, and U. Kleinekathöfer, Chebyshev Expansion Applied to Dissipative Quantum Systems, *J. Phys. Chem. A* **120**, 3270 (2016).
- [14] T. Banerjee and N. Makri, Quantum-Classical Path Integral with Self-Consistent Solvent-Driven Reference Propagators, *J. Phys. Chem. B* **117**, 13357 (2013).
- [15] R. Lambert and N. Makri, Quantum-classical path integral. I. Classical memory and weak quantum nonlocality, *J. Chem. Phys.* **137**, 22A552 (2012).
- [16] R. Lambert and N. Makri, Quantum-classical path integral. II. Numerical methodology, *J. Chem. Phys.* **137**, 22A553 (2012).
- [17] P. L. Walters and N. Makri, Quantum-Classical Path Integral Simulation of Ferrocene-Ferrocenium Charge Transfer in Liquid Hexane, *J. Phys. Chem. Lett.* **6**, 4959 (2015).
- [18] P. L. Walters and N. Makri, Iterative quantum-classical path integral with dynamically consistent state hopping, *J. Chem. Phys.* **144**, 044108 (2016).
- [19] N. Makri and D. E. Makarov, Tensor propagator for iterative quantum time evolution of reduced density matrices. I. Theory, *J. Chem. Phys.* **102**, 4600 (1995).
- [20] N. Makri and D. E. Makarov, Tensor propagator for iterative quantum time evolution of reduced density matrices. II. Numerical methodology, *J. Chem. Phys.* **102**, 4611 (1995).
- [21] N. Makri, Blip decomposition of the path integral: Exponential acceleration of real-time calculations on quantum dissipative systems, *J. Chem. Phys.* **141**, 134117 (2014).
- [22] N. Makri, Blip-summed quantum-classical path integral with cumulative quantum memory, *Faraday Discuss.* **195**, 81 (2016).
- [23] N. Makri, Iterative blip-summed path integral for quantum dynamics in strongly dissipative environments, *J. Chem. Phys.* **146**, 134101 (2017).
- [24] A. Strathearn, P. Kirton, D. Kilda, J. Keeling, and B. W. Lovett, Efficient non-Markovian quantum dynamics using time-evolving matrix product operators, *Nat. Commun* **9**, 10.1038/s41467-018-05617-3 (2018).
- [25] M. R. Jørgensen and F. A. Pollock, Exploiting the Causal Tensor Network Structure of Quantum Processes to Efficiently Simulate Non-Markovian Path Integrals, *Phys. Rev. Lett.* **123**, 10.1103/physrevlett.123.240602 (2019).
- [26] D. Gribben, A. Strathearn, J. Iles-Smith, D. Kilda, A. Nazir, B. W. Lovett, and P. Kirton, Exact quantum dynamics in structured environments, *Phys. Rev. Res.* **2**, 10.1103/physrevresearch.2.013265 (2020).
- [27] E. Ye and G. K.-L. Chan, Constructing tensor network influence functionals for general quantum dynamics, *J. Chem. Phys.* **155**, 044104 (2021).
- [28] A. Bose and P. L. Walters, A tensor network representation of path integrals: Implementation and analysis, arXiv pre-print server (2021).
- [29] A. Bose, A Pairwise Connected Tensor Network Representation of Path Integrals, arXiv pre-print server (2021).
- [30] J. Ren, Z. Shuai, and G. Kin-Lic Chan, Time-Dependent Density Matrix Renormalization Group Algorithms for Nearly Exact Absorption and Fluorescence Spectra of Molecular Aggregates at Both Zero and Finite Temperature, *J. Chem. Theory Comput.* **14**, 5027 (2018).
- [31] N. Makri, Communication: Modular path integral: Quantum dynamics via sequential necklace linking, *J. Chem. Phys.* **148**, 101101 (2018).
- [32] N. Makri, Modular path integral methodology for real-time quantum dynamics, *J. Chem. Phys.* **149**, 214108 (2018).
- [33] S. Kundu and N. Makri, Modular path integral for discrete systems with non-diagonal couplings, *J. Chem. Phys.* **151**, 074110 (2019).
- [34] S. Kundu and N. Makri, Modular path integral for finite-temperature dynamics of extended systems with intramolecular vibrations, *J. Chem. Phys.* **153**, 044124 (2020).
- [35] A. Leroze, M. Sonner, and D. A. Abanin, Influence Matrix Approach to Many-Body Floquet Dynamics, *Phys. Rev. X* **11**, 10.1103/physrevx.11.021040 (2021).
- [36] M. Fishman, S. R. White, and E. M. Stoudenmire, The ITensor Software Library for Tensor Network Calculations, arXiv pre-print server (2020).
- [37] A. O. Caldeira and A. J. Leggett, Path integral approach to quantum Brownian motion, *Physica A: Statistical Mechanics and its Applications* **121**, 587 (1983).
- [38] N. Makri, The Linear Response Approximation and Its

- Lowest Order Corrections: An Influence Functional Approach, *J. Phys. Chem. B* **103**, 2823 (1999).
- [39] A. J. Daley, C. Kollath, U. Schollwöck, and G. Vidal, Time-dependent density-matrix renormalization-group using adaptive effective Hilbert spaces, *J. Stat. Mech. Theory Exp.* **2004**, P04005 (2004).
- [40] G. Vidal, Efficient Simulation of One-Dimensional Quantum Many-Body Systems, *Phys. Rev. Lett.* **93**, 040502 (7).
- [41] M. P. Zaletel, R. S. K. Mong, C. Karrasch, J. E. Moore, and F. Pollmann, Time-evolving a matrix product state with long-ranged interactions, *Phys. Rev. B* **91**, 165112 (4).
- [42] J. Haegeman, J. I. Cirac, T. J. Osborne, I. Pizorn, H. Verschelde, and F. Verstraete, Time-Dependent Variational Principle for Quantum Lattices, *Phys. Rev. Lett.* **107**, 070601 (2011).
- [43] R. Orús, A practical introduction to tensor networks: Matrix product states and projected entangled pair states, *Ann. Phys. (N. Y.)* **349**, 117 (2014).
- [44] M. Yang and S. R. White, Time-dependent variational principle with ancillary Krylov subspace, *Phys. Rev. B* **102**, 094315 (2020).
- [45] N. Makri, Small matrix modular path integral: Iterative quantum dynamics in space and time, *Phys. Chem. Chem. Phys.* **23**, 12537 (2021).
- [46] M. V. Rakov and M. Weyrauch, Spin- $\frac{1}{2}$ XXZ Heisenberg chain in a longitudinal magnetic field, *Phys. Rev. B* **100**, 134434 (10).